Title

Facile synthesis and surface modification of bioinspired nanoparticles from quercetin for drug delivery

Journal

Biomaterials Science, 6(10)

ISSN

2047-4830

Authors

Sunoqrot, Suhair
Al-Shalabi, Eveen
Messersmith, Phillip B

Publication Date

2018-09-25

DOI

10.1039/c8bm00587g

Peer reviewed

HHS Public Access

Author manuscript

Biomater Sci. Author manuscript; available in PMC 2019 September 25.

Published in final edited form as:

Biomater Sci. 2018 September 25; 6(10): 2656–2666. doi:10.1039/c8bm00587g.

Facile Synthesis and Surface Modification of Bioinspired Nanoparticles from Quercetin for Drug Delivery†

Suhair Sunoqrot[a,b,*], **Eveen Al-Shalabi**[a], and **Phillip B. Messersmith**[b,c,d]

[a]Department of Pharmacy, Faculty of Pharmacy, Al-Zaytoonah University of Jordan, Amman 11733, Jordan

[b]Department of Bioengineering, University of California, Berkeley, CA 94720, USA

[c]Department of Materials Science and Engineering, University of California, Berkeley, CA 94720, USA

[d]Materials Sciences Division, Lawrence Berkeley National Laboratory, Berkeley, CA 94720, USA

Abstract

Nanoparticle-mediated drug delivery has demonstrated great potential to treat various diseases especially cancer. However, there is an unmet need for the scalable synthesis of multifunctional nanoparticles to meet the complex challenges of drug delivery. Here we show that we can synthesize nanoparticles from the polyphenol quercetin, which can be conveniently functionalized with ligands and drug molecules by simple mixing under ambient conditions. Nanoparticles (~30-40 nm in diameter) were formed by oxidative self-polymerization of quercetin in alkaline buffer (pH 9). The reactivity of oxidized polyphenols was exploited to immobilize amine-terminated methoxy poly(ethylene glycol) on the nanoparticles' surface for steric stability, followed by loading with doxorubicin as a model drug. Surface modification of the nanoparticles was confirmed by X-ray Photoelectron Spectroscopy. An antioxidant assay showed that the nanoparticles retained some antioxidant activity. The nanoparticles were readily internalized by KB cells *via* an endo-lysosomal pathway. Doxorubicin-loaded nanoparticles showed a drug loading of 35.6 ± 4.9 %w/w with a loading efficiency of 88.9 ± 12.4 %, sustained drug release, and potent cytotoxicity *in vitro*. Our findings demonstrate a promising new application for naturally occurring polyphenols as a renewable source of drug delivery nanocarriers that can be synthesized at low cost with minimal equipment.

TOC entry

†Electronic Supplementary Information (ESI) available: NMR, FT-IR, and UV-Vis spectra, survey and high resolution XPS spectra, and CLSM images of KB cells

*Corresponding Author: Suhair Sunoqrot, PhD, Assistant Professor of Pharmaceutics, Department of Pharmacy, Faculty of Pharmacy, Al-Zaytoonah University of Jordan, P.O. Box 130, Amman 11733, Jordan, Phone: +962-6-4291511 Ext. 312, Fax: +962-6-4291432, suhair.sunoqrot@zuj.edu.jo.

Conflicts of interest

There are no conflicts to declare.

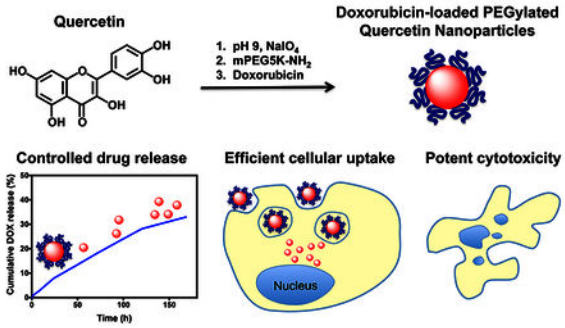

Bioinspired surface-modifiable nanoparticles are synthesized from Quercetin by oxidative self-polymerization as a promising nanoscale platform for drug delivery

Keywords

polyphenols; quercetin; bioinspired nanoparticles; surface modification; doxorubicin; PEGylation

Introduction

The application of nanotechnology in medicine has caused a paradigm shift in the treatment and diagnosis of many diseases, particularly cancer. Small molecule anti-cancer drugs are systemically distributed to tumor and normal cells alike, leading to significant side effects that can be as devastating as the disease itself. Nanoscale therapeutics enable targeted drug delivery by preferentially accumulating in tumors through the enhanced permeability and retention (EPR) effect, thus minimizing the interactions of anti-cancer drugs with healthy tissues.[1] The first generation of nanocarriers to be developed for medical applications included liposomes and polymer-drug conjugates. Since then, other nanocarrier types such as antibody-drug conjugates, polymeric nanoparticles (NPs), and polymeric micelles have also been developed with the potential to overcome the many challenges of drug delivery.[2]

To maximize drug delivery to tumors by passive targeting, which relies on the EPR effect, a nanocarrier needs to evade the body's clearance mechanisms and circulate in the blood long enough to reach its target.[3–5] This is often achieved by decorating the nanocarrier surface with hydrophilic polymers such as poly(ethylene glycol) (PEG).[6, 7] The surface can also be modified with targeting ligands to impart active targeting capabilities, which further enhances the nanocarrier's targeting efficacy.[8–11] Newer generations of nanocarriers are now leaning towards more complex features such as stimuli-responsiveness and combination therapy.[12] Although such modifications have the potential to improve their delivery efficacy, these rather complex systems will be faced with several hurdles en route to clinical translation and commercialization. Challenges such as synthesis, characterization, scale-up, and increased costs must all be addressed for these systems to be advanced forward. Thus, there is an unmet need to develop a simple, cost-effective synthesis method for next generation nanocarriers.

The catechol-rich composition of mussel adhesive proteins has inspired the development of a simple and versatile surface modification technique.[13] This surface coating method relies on

self-polymerization of catechols such as dopamine and other polyphenols in mild alkaline solutions to form thin surface-adherent films onto a wide range of substrates, mimicking the adhesion phenomena observed in mussels.[14–16] The polymerized catechol films have been shown to form a conformal layer on a variety of inorganic and organic substrates. These coatings can also serve as primers for ligand incorporation due to their propensity to covalently react with nucleophiles such as amines and thiols, as well as interact with other functionalities through hydrogen bonding, π-π stacking, and metal coordination.[17] Catechol polymerization has also contributed to the development of polydopamine- and other polyphenol-coated polymeric NPs to immobilize various ligands on the NP surface without the need for coupling reagents or complex reactions.[18–21] In addition, standalone polydopamine NPs have successfully been synthesized as promising cancer-targeted imaging and photothermal agents.[22, 23] However, with the exception of dopamine, tannic acid,[20, 24] and green tea extracts,[25–27] polyphenols have not yet been adequately explored for NP drug delivery, either as an intermediate coating layer on the NP surface for ligand immobilization, or as the NP platform itself.

Flavonoids are a family of more than 4000 naturally occurring plant polyphenolic compounds that have been widely investigated for a variety of biological activities, including anti-oxidant, cardioprotective, anti-inflammatory, and anti-cancer activities.[28] A leading example is quercetin (QCT), a polyphenol characterized by the presence of a catechol moiety. This structural feature led us to hypothesize that QCT can undergo self-polymerization in mild alkaline conditions to form colloidal aggregates. These NPs can then be conveniently modified with ligands and drug molecules in a simple procedure analogous to previously reported polyphenol coating and polydopamine NP surface functionalization methods. To test this hypothesis, we first investigated the ability of QCT to form NPs in an aqueous alkaline buffer. We functionalized the NPs with PEG as an antifouling polymer and to impart steric stability, and then conducted a series of *in vitro* experiments to evaluate their use as a prospective class of organic multifunctional NPs for drug delivery. We show by dynamic light scattering (DLS), transmission electron microscopy (TEM), and X-ray photoelectron spectroscopy (XPS) that QCT forms spherical NPs upon polymerization, and that PEG can be successfully immobilized on polyQCT (pQCT) NPs. We demonstrate that cellular uptake of PEGylated NPs occurs *via* an endocytotic pathway. We also show that PEGylated NPs can be efficiently loaded with doxorubicin (DOX) as a model drug, and that drug-loaded NPs exhibit sustained release and potent cytotoxicity *in vitro*.

Experimental

Materials

Quercetin hydrate (> 95%) (QCT) was obtained from Acros Organics (New Jersey, USA), bicine, Triton X-100, dimethylsulfoxide (DMSO), 2,2-diphenyl-1-picrylhydrazyl (DPPH), aluminum chloride ($AlCl_3$), hydrochloric acid (HCl, 10 N), and sodium methoxide (NaOMe) were obtained from Sigma-Aldrich (St. Louis, MO, USA). Sodium metaperiodate ($NaIO_4$) was provided by Alfa Aesar (Ward Hill, MA, USA), doxorubicin hydrochloride (DOX) was purchased from LC Laboratories (Woburn, MA, USA), and fluorescein isothiocyanate (FITC) isomer I was obtained from Chem-Impex International Inc. (Wood Dale, IL, USA).

Methoxy poly(ethylene glycol) 5000 amine (mPEG5K-NH_2) and poly(ethylene glycol) 5000 diamine (NH_2-PEG5K-NH_2) were provided by Laysan Bio (Arab, AL, USA), glacial acetic acid was purchased from Fisher Scientific (Pittsburg, PA, USA), and sodium acetate was obtained from Spectrum Chemical Manufacturing Corp. (Gardena, CA, USA). Phosphate buffered saline (PBS) was obtained from Mediatech (Manassas, VA, USA), and ultrapure Milli-Q water (specific resistivity ~18.2 MΩcm at 25 °C) was prepared using a water purification system (EMD Millipore, Billerica, MA, USA).

Synthesis of pQCT NPs

pQCT NPs were synthesized by oxidative self-polymerization in mild alkali, analogous to polydopamine NP synthesis.[23] Briefly, QCT (20 mg, 6.6×10^{-5} mol) was dissolved in 2 mL of 25% DMSO in 0.1 M bicine buffer pH 9, to which $NaIO_4$ (14 mg, 6.6×10^{-5} mol) was immediately added and vigorously stirred at room temperature (RT) overnight. NPs were then purified by ultrafiltration using Amicon Ultra-15 centrifugal filter units with MWCO 100,000 (EMD Millipore, Billerica, MA, USA) at 4000 rpm for 15 min (Sorvall Legend X1R centrifuge, Thermo Scientific, Waltham, MA, USA), to remove large aggregates. The filtrate was then further purified to remove unreacted QCT and any remaining impurities by ultrafiltration using Amicon Ultra-15 centrifugal filter units with MWCO 10,000 under the same centrifuge settings as above, and repeated washing with Milli-Q water at least 5 times. pQCT NPs were then resuspended in 1 mL Milli-Q water and stored at 4 °C until use.

Characterization by NMR, FT-IR, and UV-Vis spectroscopy

NMR spectra for QCT and pQCT were recorded in DMSO-d_6 using a Bruker Avance III 500 MHz spectrometer (Billerica, MA, USA). FT-IR spectra were recorded using a Shimadzu IR Affinity-1 spectrometer (Kyoto, Japan), where all samples were prepared as KBr discs. UV-Vis spectroscopy was used to determine the presence of free -OH groups using NaOMe and $AlCl_3$/HCl as shift reagents.[29, 30] First, the spectra of QCT and pQCT (10 μg/mL in methanol) were recorded. Three drops of 1 M NaOMe methanolic solution was then added to each sample and the spectra were immediately recorded. The $AlCl_3$ spectrum was recorded immediately after adding 6 drops of 50 mg/mL $AlCl_3$ methanolic solution to another sample of QCT and pQCT. The $AlCl_3$/HCl spectrum was recorded immediately after adding 3 drops of 5 N HCl to the $AlCl_3$ samples. All analyses were performed using a Shimadzu UV-1800 spectrometer (Kyoto, Japan).

Synthesis of FITC-PEG5K-NH_2

One hundred milligrams (2×10^{-5} mol) of NH_2-PEG5K-NH_2 was dissolved in 10 mL DMSO, to which FITC (7.8 mg, 2×10^{-5} mol) was added under vigorous stirring in the dark at RT overnight. Unreacted FITC was removed by membrane dialysis (Slide-A-Lyzer cassette, MWCO 3500, Thermo Fisher Scientific, Waltham, MA, USA) against 4 L deionized (DI) water with frequent water changes over 4 days. FITC-PEG5K-NH_2 was then lyophilized (Labconco FreeZone 4.5 Plus, Kansas City, MO, USA) and stored at −20 °C until use. Successful FITC conjugation was confirmed by ^{1}H-NMR (Bruker Avance AVB-400, Billerica, MA, USA) in D_2O (Figure S1). The number of FITC molecules per PEG chain was calculated by UV-Vis (Shimadzu UV-2600 spectrometer, Kyoto, Japan) in Milli-Q water at 488 nm, and was found to be 0.9 FITC/PEG.

Synthesis of pQCT@PEG and pQCT@FITC-PEG NPs

PEGylated pQCT NPs were prepared as previously described for polydopamine NPs.[23] Briefly, 0.5 mL pQCT NPs prepared above were diluted up to 2 mL in 0.1 M bicine buffer pH 9. mPEG5K-NH_2 (50 mg) was added to the solution of pQCT NPs in bicine to achieve a final concentration of 5 mM. The solution was vigorously stirred at RT overnight, followed by removal of unreacted mPEG5K-NH_2 and buffer by ultrafiltration and repeated washing with Milli-Q water under the same conditions described for pQCT NP synthesis. pQCT@PEG NPs were resuspended in 1 mL Milli-Q water, lyophilized, and stored at −20 °C until use. For the synthesis of FITC-labeled NPs, NPs diluted in up to 2 mL bicine buffer pH 9 were first mixed with 5 mg FITC-PEG5K-NH_2 for 3 h, followed by adding 45 mg mPEG5K-NH_2 to the buffer solution. The resulting pQCT@FITC-PEG NPs were purified by ultrafiltration as described above.

Preparation of pQCT@PEG@DOX and pQCT@FITC-PEG@DOX NP

pQCT@PEG NPs were loaded with DOX as a model drug and as a fluorescent probe by dissolving 5 mg lyophilized NPs in 1 mL bicine buffer pH 9 containing 2.5 mg DOX. The mixture was stirred vigorously overnight at RT protected from light. Excess DOX was removed by ultrafiltration and repeated washing with Milli-Q water as described above, except that the filter units were pre-soaked in 5% Triton-X 100 for 2 h to minimize DOX adsorption to the filter. The resulting pQCT@PEG@DOX NPs were redispersed in 1 mL Milli-Q water and lyophilized for further use. DOX loading was measured by dissolving a known amount of NPs in Milli-Q water and measuring the UV absorbance at 490 nm, based on a calibration curve of DOX in Milli-Q water at 490 nm. Each measurement was repeated at least three times using different batches of NPs. Drug loading and loading efficiency were calculated according to Equations (1) and (2), respectively:

$$\text{Drug loading}(\%\,\text{w}/\text{w}) = (\text{Actual weight of DOX in NPs} / \text{Weight of NPs}) \times 100\,\% \quad (1)$$

$$\text{Loading efficiency}(\%) = (\text{Actual weight of DOX in NPs} / \text{Theoretical weight of DOX in NPs}) \times 100\,\% \quad (2)$$

For the preparation of dual-labeled NPs, pQCT@FITC-PEG NPs were loaded with DOX using the same procedure described above for pQCT@PEG NPs.

Differential scanning calorimetry (DSC) analysis

The thermograms of QCT, pQCT. pQCT@PEG NPs, pQCT@PEG@DOX NPs, pQCT@PEG/DOX physical mixture, and DOX were recorded using a DSC 1 STARe System (Mettler Toledo, Columbus, OH, USA). Approximately 1 mg of each sample was heated in an aluminum pan from 25 – 350 °C and the scanning rate was conducted at 10 °C/min.

Particle size and zeta potential measurements

Particle size and zeta potential of the NPs prepared in this study were measured by DLS using a Zetasizer Nano ZS (Malvern, UK) at a measurement angle of 173°. NPs were dispersed in Milli-Q water for size measurements and PBS pH 7.4 for zeta potential measurements at a concentration of 1 mg/mL. To verify steric stability of the NPs after PEGylation, NPs were dispersed in GIBCO RPMI 1640 cell culture medium (Invitrogen, Carlsbad, CA, USA) supplemented with 10% fetal bovine serum (FBS, Invitrogen) and incubated at RT for 24 h prior to the measurement. Each measurement was performed at least three times using different batches of NPs.

Preparation of samples for TEM

A drop of each NP suspended in Milli-Q water was placed on carbon-coated copper grids for 1 min. Excess liquid was wicked with filter paper and the grids were stored in a vacuum dessicator. Grids were imaged using a Philips Tecnai 12 TEM (FEI, Hillsboro, OR, USA) at an accelerating voltage of 120 kV.

XPS analysis

Successful PEGylation of pQCT NPs was verified by XPS. Briefly, TiO_2-coated silicon substrates were cleaned by consecutive sonication in Milli-Q water, acetone, and isopropanol for 10 min each, followed by drying under a stream of N_2 and then plasma discharge (Harrick Plasma Cleaner, Ithaca, NY, USA) at 60 W for 5 min. A drop of each NP suspension was then placed onto the surface of the substrates and left to dry overnight. Substrates were completely dried under vacuum prior to analysis using a PHI 5600 spectrometer (PerkinElmer, Waltham, MA, USA) equipped with an Al monochromated 2 mm filament and a built-in charge neutralizer. The X-ray source operated at 350 W power and 15.0 V voltage. Survey scans were performed between 0 and 1200 eV electron binding energies. High resolution spectra of the C 1s, N 1s, and O 1s regions were obtained between 280 – 305, 395 – 410, and 525 – 535 eV, respectively. Charge correction was performed by setting the C 1s peak at 285 eV. Data analysis was conducted using MultiPak software version 9.6.015.

Antioxidant activity of pQCT and pQCT@PEG NPs

DPPH radical scavenging activity of pQCT NPs and pQCT@PEG NPs compared to QCT was tested as previously reported.[31] For the assay, 0 – 1000 μg of each material was dissolved in 200 μL ethanol (QCT) or Milli-Q water (pQCT and pQCT@PEG NPs). The solutions were immediately added to 4 mL DPPH (0.1 mM in ethanol) and incubated at RT in the dark for 30 min. The absorbance of the solutions was then measured at 517 nm using an Infinite M200 Tecan microplate reader (Männedorf, Switzerland). Scavenging activity (I) was calculated according to Equation (3):

$$I = [1 - (A_t - A_b) / A_c] \times 100\,\% \quad (3)$$

where A_t is the absorbance of each test material upon incubation with DPPH, A_b is the background absorbance of each test material without DPPH, and A_c is the absorbance of DPPH alone.

Cellular uptake of pQCT@FITC-PEG NPs

The KB cell line (ATCC, Manassas, VA, USA) was used as a model human cancer cell line throughout this study. Cells were grown as a monolayer at 37 °C and 5% CO_2 in GIBCO RPMI 1640 medium (Invitrogen) supplemented with penicillin (100 units/mL), streptomycin (100 mg/mL), and 10% heat-inactivated FBS (Invitrogen). For the cellular uptake study, cells were seeded in 4-well chamber slides (Millicell EZ Slide, Millipore, Billerica, MA, USA) at a density of 2.0×10^5 cells/well and incubated in complete RPMI 1640 for 24 h. Cells were then treated with 500 μL of 10 μg/mL pQCT@FITC-PEG NPs dispersed in basal RPMI 1640 for 1, 3, 6, and 24 h. At the end of each incubation time, cells were washed with PBS three times, and then stained with LysoTracker™ Red DND-99 (LTR, 100 nM in PBS, Invitrogen) for 30 min at 37 °C. After the staining, cells were washed once with PBS and then fixed in 4% paraformaldehyde (Santa Cruz Biotech, Dallas, TX, USA) for 10 min at RT. The fixed cells were washed twice with PBS and then mounted with ProLong™ Gold antifade reagent with DAPI (Invitrogen) and covered with glass cover slips. Cellular uptake was visualized using a Zeiss LSM 710 confocal laser scanning microscope (CLSM, Carl Zeiss GmbH, Gena, Germany). The 405 and 488 nm lines of a diode laser were used for the excitation of DAPI and FITC, respectively, and the 543 nm line of a HeNe laser was used for the excitation of LTR. Emission was filtered between 410 – 492 nm for DAPI, 493 – 534 nm for FITC, and 559 – 674 nm for LTR. Images were captured using a W Plan-Apochromat 63×/1.0 objective, and were acquired at a box size of 1024 × 1024 pixels, a scan speed of 5 fps (1.58 μs/pixel), and an average line scan of 4. All obtained images were processed using Zen software (Carl Zeiss). Colocalization of FITC with LTR was measured based on Pearson's correlation coefficient calculated using ImageJ 1.51m9 (NIH, Bethesda, MD, USA), where a value between 0 and +1 indicates positive correlation.

For flow cytometry analysis, KB cells were seeded in 12-well plates at a density of 1.0×10^6 cells/well in RPMI 1640 for 24 h. Cells were then treated with the NPs (1 mL of 10 μg/mL solution in basal RPMI 1640) for 3 h at 37 and 4 °C. After the treatment, cells were washed three times with PBS and then suspended with TrypLE™ Express (Invitrogen). Cell suspensions were centrifuged at 3500 rpm for 5 min, the cells were resuspended in 200 μL 1% paraformaldehyde, and then transferred to U-bottom 96-well plates. The fluorescence signal intensities from the samples were measured using an Attune NxT Flow Cytometer (Thermo Fisher Scientific) equipped with a microplate autosampler, and data analysis was performed using the accompanying software.

In vitro release of DOX from pQCT@PEG@DOX NPs

The release test was performed as previously described.[32] Briefly, 1 mg samples of pQCT@PEG@DOX NPs were placed in microcentrifuge tubes in triplicate and dispersed in 1 mL of either PBS pH 7.4 or acetate buffer pH 5.0, and then placed in an orbital shaking water bath incubator (GFL 1083, Burgwedel, Germany) operating at 100 rpm and 37 °C. Samples were periodically withdrawn from the release medium and centrifuged (Hettich

EBA 12 Zentrifugen, Tuttlingen, Germany) at 20,000 × g for 15 min. Nine hundred microliters of the supernatant containing the released drug was removed and replaced with an equal volume of the appropriate buffer. The NP pellets were then redispersed and the samples placed back in the incubator. The amount of DOX released at each time point was calculated by measuring the UV absorbance of the samples at 482 nm using a Shimadzu UV-1800 spectrometer (Kyoto, Japan), based on a calibration curve of DOX absorbance in each buffer. The results were plotted as cumulative % amount of DOX released versus time.

Cellular uptake of pQCT@FITC-PEG@DOX NPs

KB cells were seeded in 4-well chamber slides at a density of 2.0×10^5 cells/well in complete RPMI 1640 for 24 h. Cells were then treated with 5 μM free DOX or an equivalent concentration of DOX in pQCT@FITC-PEG@DOX NPs diluted in basal RPMI 1640 for 1, 3, 6, and 24 h. At each time point, cells were washed with PBS, fixed in 4% paraformaldehyde, mounted with the antifade agent, and then observed under CLSM as described above for pQCT@FITC-PEG NPs.

Cytotoxicity of pQCT@PEG@DOX NPs

KB cells were seeded in 96-well plates at a density of 1.0×10^4 cells/well in complete RPMI 1640 for 24 h. Cells (n = 5) were then treated with free DOX or pQCT@FITC-PEG@DOX NPs at DOX concentrations ranging from 0 to 100 μM in complete RPMI 1640 for 48 h. Another set of cells was treated with pQCT@PEG NPs at concentrations ranging from 0 to 1 mg/mL. At the end of the incubation period, the medium was removed and replaced with complete RPMI 1640 (100 μL/well). Cell viability was assessed using a CellTiter 96 Aqueous One Solution (MTS) assay (Promega, Madison, WI, USA) by adding 20 μL of the reagent to each well. Cells were incubated for 2 h, and then the UV absorbance was measured at 490 nm using an Infinite M200 microplate reader. Mean cell viabilities were determined relative to a negative control (cells treated with complete RPMI 1640 only) and a positive control (cells lysed using 0.1% Triton X-100). Plots of cell viabilities vs. DOX concentration were constructed from the average of three independent experiments and used to determine IC50 for free DOX and DOX-loaded NPs.

Statistical analysis

Statistical analysis was performed in Graphpad Prism 6.0e by conducting analysis of variance (ANOVA) followed by Tukey's post-hoc test, where $p < 0.05$ was considered statistically significant.

Results

Synthesis and characterization of pQCT NPs

An overview of NP synthesis is shown in Figure 1A, and a proposed mechanism for QCT polymerization is depicted in Figure 1B. QCT undergoes oxidation in alkaline buffers, causing a change in solution color from bright yellow to amber brown. $NaIO_4$ was added to accelerate and to ensure reproducible QCT oxidation, thus limiting batch-to-batch variability. Ultrafiltration was employed to remove large aggregates (> 100,000 Da), unreacted QCT molecules, as well as small aggregates (< 10,000 Da), in order to finally

obtain water-dispersible pQCT NPs with an average yield of 75.6% and uniform size (Figure 2 and Figure 3A).

Different spectroscopic techniques were used to investigate the structure of pQCT resulting from oxidative coupling of QCT. The ^{1}H-NMR spectrum of QCT (Figure S2) showed a pair of doublets at δ 8.19 and 8.41 ppm, corresponding to ring A protons at C-6 and C-8. Ring B protons appeared at δ 9.68, 8.94, and 9.55 ppm for C-2', C-5', and C-6', respectively, which confirms that ring B is disubstituted. The downfield singlets at δ 11.29, 11.33, 11.57, 12.77, and 14.46 ppm refer to hydroxyl groups at C-7, C-3', C-4', C-3, and C-5, respectively. The ^{1}H-NMR spectrum of pQCT (Figure S3) showed similar chemical shifts to those observed for QCT, albeit with a five-fold increase in the integration values of the peaks corresponding to the aromatic protons at C-6, C-8, C-2', C-5', and C-6' between δ 7.98 – 9.68. This finding suggests that QCT oxidation and the subsequent formation of reactive quinones have likely led to the formation of oligomers comprising approximately 5 monomers randomly cross-linked through C-C or C-O coupling (Figure 1B). Interestingly, -OH protons displayed only a 2.6-fold increase in integration values compared to the same proton peaks in QCT, which can be attributed to the oxidative state of approximately 2 out of 5 -OH protons in pQCT, consistent with the formation of quinones.

The FT-IR spectrum of QCT (Figure S4) exhibited the characteristic bands corresponding to O-H stretching (3416 and 3330 cm^{-1}), C=O stretching (1668 cm^{-1}), C=C aromatic stretching (1612, 1562, and 1522 cm^{-1}), O-H bending (1382 cm^{-1}), and C-H aromatic bending (825 cm^{-1}). The spectrum of pQCT showed similar peaks, indicating that no new functional groups were formed after oxidation and polymerization.

The UV-Vis spectra of QCT and pQCT in methanol before and after the addition of NaOMe, $AlCl_3$, and $AlCl_3$/HCl were used to determine the oxidation state of QCT before and after polymerization.[29, 30, 33] As depicted in Figure S5, QCT shows absorption bands at 256 nm (band II) and 371 nm (band I). A bathochromic shift to 422 nm for band I was observed after adding NaOMe, which confirms the presence of a free -OH group at C-3. In addition, the appearance of a new peak at 327 nm indicates the presence of a free -OH group at C-7. A bathochromic shift to 428 for band I upon the addition of $AlCl_3$/HCl confirmed the presence of free -OH groups on C-3 and C-5. A bathochromic shift to 457 nm for band I was observed upon the addition of $AlCl_3$, which was greater than that in $AlCl_3$/HCl by 29 nm, indicating the presence of *o*-dihydroxyl groups on ring B. On the other hand, the UV-Vis spectrum of pQCT showed absorption bands at 300 nm for band II and 348 nm for band I. A 70 nm bathochromic shift to 418 nm for band I was observed after the addition of NaOMe, confirming the presence of a free -OH group at C-3. The appearance of a new peak at 329 nm indicates the presence of a free -OH group at C-7. A bathochromic shift of 74 nm to 422 nm for band I was observed after adding $AlCl_3$, but was not affected by the addition of HCl. This confirms the presence of free -OH groups on C-3 and C-5, and the absence of *o*-dihydroxyl groups on ring B, which signifies that the catechol groups on ring B have been oxidized to quinones, making them unavailable for complexation with $AlCl_3$ (Figure S5).

Taken together, spectroscopic analyses of pQCT strongly suggest that QCT oxidation led to the formation of reactive quinones on ring B capable of undergoing nucleophilic addition

reactions, resulting in larger MW oligomers composed of approximately five monomers. Given that pQCT was ultrafiltered through a 10,000 MWCO membrane, which is larger than the MW of 5 QCT monomers (~1,500 Da), most likely the oligomers underwent further self-assembly forming colloidal aggregates larger than 10,000 Da, as proposed in Figure 1B.

pQCT NPs were PEGylated by simple mixing under ambient conditions with mPEG-NH_2, which was employed both as a model ligand and for steric stabilization. The FT-IR spectrum of pQCT@PEG NPs (Figure S4) exhibited the characteristic C-H and C-O-C stretching bands at 2889 cm^{-1} and 1110 cm^{-1}, respectively. As shown in Figure 2 and Figure 3A, PEGylation did not lead to a significant increase in NP size as previously reported for polydopamine NPs.[23] This may be related to the PEG grafting density and suggests that the PEG chains exist in a mushroom conformation on the NP surface.[34] NP size also remained unchanged after loading with DOX (Figure 2 and Figure 3A). Although pQCT NPs were completely soluble in MilliQ water (Figure 2B), around 2-fold increase in NP size was observed upon incubation of pQCT NPs in cell culture medium containing 10% FBS, which may be attributed to NP aggregation and/or surface adsorption of serum proteins (Figure 3A). Particle size of PEGylated NPs with or without DOX in the presence of serum proteins remained unchanged, which verifies steric stability imparted by PEG (Figure 3A).

Zeta potential of the NPs was measured in PBS at pH 7.4. As shown in Figure 3B, pQCT NPs exhibited a negative potential of −14.9 ± 3.0 mV. This value was significantly decreased upon PEGylation to −3.1 ± 2.9 and −2.4 ± 1.3 mV for pQCT@PEG and pQCT@PEG@DOX NPs, respectively, further confirming successful and stable surface modification of pQCT NPs with PEG even after DOX loading.

XPS was employed to further verify NP surface composition. As shown in Table 1, pQCT NPs were characterized by a C/O ratio of 2.15, which is very close to the theoretical ratio of 2.14. PEGylation resulted in a decrease in the C/O ratio to 1.85. Survey and high resolution spectra of modified pQCT NPs indicated the presence of N 1s signals that were significantly higher ($p < 0.05$) than unmodified NPs (Figure S6), corroborating successful surface functionalization of the NPs with mPEG-NH_2. Additionally, high resolution spectra of the C 1s and O 1s regions revealed large increases in C-O components in pQCT@PEG and pQCT@PEG@DOX NPs, attributed to the presence of PEG on the NP surface (Figure S7). pQCT@PEG@DOX NPs displayed a slightly higher N % than pQCT@PEG NPs, attributed to the primary amine found in DOX. Overall, NP characterization by TEM, DLS, zeta potential, and XPS confirm that we have successfully synthesized spherical pQCT NPs which were subsequently modified with PEG and DOX.

Antioxidant activity of pQCT NPs

A DPPH assay was conducted comparing the scavenging activity of pQCT and pQCT@PEG NPs to unmodified QCT. As depicted in Figure 4, QCT is a potent antioxidant, with 25 μg causing 81.3% reduction in the formation of DPPH radicals, and 97.4% quenching at 125 μg. On the other hand, pQCT NPs exhibited a marked decrease in their antioxidant activity, with 65.7% scavenging activity observed at 125 μg and 88.8% at 1000 μg. Therefore, antioxidant activity of pQCT NPs was not completely diminished, indicating that some phenolic groups were still in their reduced form even after NP formation by oxidative self-

polymerization. Antioxidant activity was also observed for pQCT@PEG NPs. However, it was significantly lower than unmodified NPs (41.6% and 72.7% scavenging activity corresponding to 125 and 1000 μg, respectively). This could be attributed to the fact that the same mass of pQCT@PEG NPs contains a lower content of pQCT than unmodified NPs. In addition, conjugation of mPEG-NH_2 to the oxidized catechol moieties of pQCT NPs would consequently make them unavailable to act as free radical scavengers.

Cellular uptake and intracellular fate of pQCT@FITC-PEG NPs

Figure 5A shows CLSM images of KB cells after 24 h of incubation with FITC-labeled NPs (the complete set of images spanning 1 – 24 h incubation are depicted in Figure S8). We observed time-dependent uptake of the NPs, most likely through an endo-lysosomal pathway, which was confirmed by colocalization of the NP signals (green channel) with those of LTR (red channel) (Pearson's correlation coefficient = 0.71). Our observations were further corroborated by incubating the cells with the NPs at 4 °C to slow down/block endosomal trafficking.[35] As demonstrated in Figure 5B, cellular uptake was significantly reduced after 3 h incubation at 4 °C, signifying that it most likely occurred through an endolysosomal pathway.

Loading and sustained release of DOX from pQCT@PEG@DOX NPs

DOX loading was conducted under similar conditions as PEGylation, i.e. in aqueous buffer at pH 9 and mixing overnight. The resultant NPs were found to contain on average 35.6 ± 4.9 % w/w DOX. In addition, loading efficiency was found to be 88.9 ± 12.4 %, which indicates the high affinity and compatibility between DOX and pQCT NPs. The interaction between pQCT NPs and DOX was further probed by FT-IR, UV-Vis, and DSC. The FT-IR spectrum of DOX and DOX-loaded NPs (Figure S4) showed no significant changes in the characteristic peaks of DOX after loading. On the other hand, the UV-Vis spectrum of DOX-loaded NPs (Figure S9) exhibited a red shift in λ_{max} to 490 nm compared to that of the free drug (482 nm). This shift may be attributed to the interactions between the two materials.

Thermal analysis by DSC (Figure S10) showed that QCT was in a crystalline state, exhibiting two sharp endothermic peaks at 136.2 and 316.3 °C, corresponding to water evaporation and melting, respectively. pQCT displayed no characteristic thermal transitions, indicating the amorphous nature of the material. The thermogram of pQCT@PEG showed an endothermic peak at 55.7 °C, corresponding to the glass transition of PEG chains. This peak was shifted to 51.7 °C and attenuated in pQCT@PEG@DOX NPs, signifying interaction with DOX. DOX was in a crystalline state, exhibiting an endothermic melting peak at 208.3 °C, and an exothermic peak attributed to thermal degradation at 258.3 °C, which were both absent in the thermogram of DOX-loaded NPs. These changes are a strong indicator of the presence of interactions between DOX and pCT NPs, which led to changes in the structural organization of the molecules in the solid state. These interactions are likely the result of H-bonding and π-π stacking, as suggested by the structures of DOX and pQCT NPs. This result also indicates that DOX was present in the NPs in an amorphous state.

Drug release was studied under physiologically relevant conditions at pH 7.4. Drug release was also studied at pH 5.0 to simulate the acidic pH of lysosomes, since CLSM images of

FITC-labeled NPs had revealed their cellular uptake through an endo-lysosomal pathway. As depicted in Figure 6, DOX was gradually released from the NPs over the period of the study, with 47.1% of the loaded amount released in PBS pH 7.4 after 24 h, and 71.6% released after 4 days. Drug release was much faster at pH 5.0, reaching 68.1% after 24 h and 70.7% after 4 days, confirming that the NPs can control the release of DOX at physiologic pH and readily release it at lysosomal pH.

Time-dependent uptake and intracellular release of DOX-loaded NPs

We incubated KB cells with DOX-loaded FITC-labeled NPs and monitored their uptake over 24 h. Representative CLSM images after 3 and 24 h incubation are shown in Figure 7, and the complete set of images spanning 1 – 24 h are summarized in Figure S11. After 3 h incubation, free DOX was readily taken up by the cells and translocated to the nucleus. pQCT@FITC-PEG@DOX NPs were internalized by KB cells more slowly that the free drug and were mainly observed in the cytoplasm (Figure 7A). The overlap of green (FITC-labeled NPs) and red (DOX) fluorescence signals in the cytoplasm and the absence of red fluorescence signals (DOX) in the nucleus signify that drug release has not yet occurred since the NPs are not expected to cross the nuclear envelope. However, after 24 h, red signals started to appear in the nucleus, indicating DOX release from the NPs, while FITC-labeled NPs remained in the cytoplasm (Figure 7B-D).

Cytotoxicity of DOX-loaded NPs

Intracellular release of DOX was further verified by evaluating the cytotoxicity of DOX-loaded NPs compared to the free drug. KB cells were treated with both groups at DOX concentrations ranging between 0 – 100 μM for 48 h to allow sufficient time for the drug to be internalized and exert its action. The dose-response curves of free DOX and DOX-loaded NPs were plotted as cell viability % vs. DOX concentration and are shown in Figure 8. Drug-free pQCT@PEG NPs were found to be nontoxic up to 1 mg/mL (Figure S12). Free DOX displayed an IC50 of 0.1 μM, while DOX-loaded NPs exhibited slightly lower potency with an IC50 of 0.9 μM. This reduction in potency was expected due to the slower drug uptake compared to the free molecule as revealed by CLSM. Nonetheless, IC50 for free DOX and NPs were within the same order of magnitude and were comparable to values reported in the literature using similar systems,[27, 36] indicating that DOX-loaded NPs were able to control the release and deliver the drug intracellularly without compromising its efficacy.

Discussion

Bioinspired polymerization of catechols has been the subject of many investigations during the last few years, mainly to produce biocompatible, versatile, and robust coatings on 2- and 3-D substrates. Polydopamine NPs were first reported by Ju *et al.*, who described the synthesis of melanin-mimetic NPs from dopamine HCl incubated at basic pH.[31] Although the exact mechanism and chemical composition of these NPs are still not fully understood, recent investigations have revealed that the process is initiated by dopamine oxidation followed by the formation of small oligomers stabilized by π–π interactions.[37] The most appealing feature of this class of coatings is their unique ability to bind a wide range of

substrates through covalent and non-covalent interactions.[13] Similarly, polydopamine NPs are able to bind various ligands more conveniently than with conventional surface modification techniques, producing multifunctional nanocarriers for a variety of applications. Dopamine has so far been the major focus of investigations for polyphenol NP synthesis. However, Nature has provided an abundant source of chemically similar compounds that can be leveraged for biomedical applications.

In this study, we set out to investigate QCT, the major representative of flavonoids, as a potential new NP platform for drug delivery. QCT is a ubiquitous polyphenol widely available from a variety of plant sources, particularly onions, kale, broccoli, and apples.[38] It can be extracted using a variety of techniques such as classic solvent extraction by heating under reflux, ultrasonic extraction, and microwave-assisted extraction.[39] The wide abundance of QCT makes it an attractive source of raw material for large scale applications. We found that QCT can undergo oxidative self-polymerization under alkaline aqueous conditions, forming spherical NPs as observed under TEM. NP formation was likely initiated upon oxidation of the catechol moieties in QCT to form reactive quinones, followed by a cascade of C-C and C-O coupling reactions that resulted in oligomers capable of forming spherical aggregates stabilized by non-covalent interactions. This proposed mechanism, which is supported by NMR and UV-Vis spectroscopy, is in agreement with the oxidation-triggered coupling reactions occurring in plant polyphenols reported by Quideau et al.[40] and described for NPs synthesized from green tea polyphenols.[25–27, 41] However, unlike these latter reports, which employed elevated temperatures and/or metal chelators for NP synthesis, our nanoscale platform was synthesized under ambient, metal-free conditions.

We showed that pQCT NPs can be efficiently PEGylated to achieve steric stability.[6] This modification step also demonstrated the ability of pQCT NPs to bind nucleophilic ligands such as mPEG-NH_2, due to the reactivity of the oxidized catechol moieties in pQCT. It has been previously reported that polyphenol coatings can readily incorporate nucleophiles bearing thiol or primary amine groups, most likely through Michael addition or Schiff base reactions.[42] Polydopamine and polyphenol-coated NPs have been modified with PEG, albumin, antibodies, and small molecule drugs *via* a similar approach.[19, 20, 23] Stability of PEGylated NPs in the presence of serum proteins, as well as the significant change observed in their zeta potential and surface elemental composition all verified successful immobilization of PEG on pQCT NPs.

QCT is among a class of compounds that are widely known for their antioxidant and free-radical scavenging activity. Given that our NP synthesis method relied on QCT oxidation, we considered the possibility that pQCT NPs might lose their antioxidant activity during synthesis. However, although it was reduced, we found that the NPs still retained significant free radical scavenging activity. This observation is consistent with a previous report involving polydopamine NPs, where 50 – 90% DPPH radical scavenging activity was observed for 100 μg of NPs depending on their particle size, despite the fact that their synthetic procedure involved oxidation.[31]

In order to evaluate pQCT NPs as a prospective drug delivery platform, it is essential to investigate their cellular interactions and intracellular trafficking. For this purpose, NPs were

labeled with FITC by adding FITC-PEG-NH_2 during PEGylation, resulting in pQCT@FITC-PEG NPs. Several mechanisms for NP entry into cells have been proposed, the most common of which is clathrin-mediated endocytosis.[43] This uptake mechanism can occur through either receptor-specific or nonspecific (adsorptive) uptake. NPs entering the cell by this route typically end up in lysosomes. When pQCT@FITC-PEG NPs were incubated with KB cells, they were mainly found in lysosomal compartments, as indicated by colocalization of their signals with LTR. The uptake mechanism of the NPs was confirmed by the significant reduction in uptake at low temperature, which has been shown to slow down and block endo-lysosomal trafficking, consistent with previous reports.[35, 44–46]

The ability of pQCT NPs to function as a drug delivery platform was validated by loading pQCT@PEG NPs with DOX. DOX is a good candidate for this purpose, as it possesses multiple aromatic rings and hydroxyl groups, which are expected to facilitate loading onto pQCT NPs through noncovalent interactions such as **π-π** stacking and H-bonding. The primary amine in DOX is not likely to have contributed to drug loading through covalent bond formation, since subsequent experiments revealed that drug release did occur. NP-drug interaction was also examined by UV-Vis and DSC, which confirmed such interactions by the observed shift in λ_{max}, the disappearance of DOX's melting peak, and the shift in the melting peak of PEG in pQCT@PEG@DOX NPs. The latter finding suggests that DOX may have formed H-bonding interactions with PEG chains as well. High drug loading and loading efficiency were consistently obtained even in the presence of PEG, indicating that DOX was able to bind to the free pQCT surface remaining after PEGylation. Similar results were obtained for PEGylated polydopamine NPs functionalized with rhodamine B and rhodamine 123, aromatic dyes containing a weak primary amine.[23]

Drug release from polymeric carriers typically follows a biphasic profile, with a burst release followed by a sustained release phase. Burst release is often attributed to desorption of surface-bound molecules, while the sustained release phase results from slow diffusion of more tightly bound and/or encapsulated molecules.[47] One potential caveat with high drug loading is burst release, which can negatively impact NP performance *in vivo*, as premature drug release can lead to nonspecific biodistribution and excretion. DOX-loaded pQCT NPs followed a sustained release profile at pH 7.4 with no burst release phase. This could be attributed to the high affinity of DOX to pQCT as indicated by the high loading achieved, and shielding of DOX molecules by the PEG corona. Sustained drug release and the lack of a burst release phase strongly suggest that the drug loading process produced stable NPs suitable for *in vivo* administration. We observed faster drug release with a burst release phase during the first 8 h in acidic buffer compared to pH 7.4, which likely promoted intracellular release in the subsequent cellular uptake experiments.

DOX-loaded NPs were readily internalized by KB cells, and after 24 h of incubation, DOX was able to escape the lysosomes and was observed in the nucleus. Intracellular drug release was also confirmed by cytotoxicity assays, which revealed that drug-loaded NPs had similar potency to the free drug after 48 h incubation. Although the exact mechanism of drug loading and release is not yet fully understood, it is evident that the low pH inside the lysosomes can accelerate the process, making the drug available to reach its intended target.

Conclusions

In this study, we tested the hypothesis that organic metal-free NPs can be synthesized from the ubiquitous flavonoid QCT by a simple mixing process under ambient conditions. Various characterization methods supported our hypothesis and demonstrated the ability of these NPs to conveniently incorporate different ligands such as PEG for steric stabilization and DOX as a therapeutic agent. PEGylation likely proceeded through covalent bond formation between the amine terminus and the reactive oxidized catechol groups of pQCT. DOX loading likely occurred *via* non-covalent (H-bonding, π-π stacking) interactions as indicated by slow drug release. Intracellular trafficking of the NPs followed predominantly an endo-lysosomal pathway, where the drug was gradually released into the cytoplasm and was able to cross the nuclear envelope to exert its action. Polyphenol NPs have previously been reported but only for dopamine and green tea polyphenol extracts.[25–27, 31, 41] Our work represents the first report on polyphenol NPs synthesized from QCT. Furthermore, these previous reports employed elevated temperatures and/or metal chelators for NP synthesis, while pQCT NPs were successfully synthesized under ambient, metal-free conditions. Ease of synthesis and surface modification of pQCT NPs makes them promising candidates as versatile drug delivery nanocarriers that can be tailored to incorporate various ligands and cargo without the need for complex coupling reactions or purification steps.

Supplementary Material

Refer to Web version on PubMed Central for supplementary material.

Acknowledgments

This work was supported by the Fulbright Visiting Scholar Fellowship awarded to SS, and in part by grant R37 DE014193 awarded to PBM. The use of the LSM 710 microscope was supported in part by the NIH S10 program under award number 1S10RR026866-01. The authors would like to thank Dr. Caroline Sugnaux from the University of California, Berkeley for assistance with XPS analysis.

References

1. Peer D, Karp JM, Hong S, Farokhzad OC, Margalit R and Langer R, Nat. Nanotechnol, 2007, 2, 751–760. [PubMed: 18654426]
2. Sunoqrot S, Hamed R, Abdel-Halim H and Tarawneh O, Curr. Topic. Med. Chem, 2017, 17, 1451–1468.
3. Maeda H, Bioconjugate Chem, 2010, 21, 797–802.
4. Bertrand N, Wu J, Xu XY, Kamaly N and Farokhzad OC, Adv. Drug Delivery Rev, 2014, 66, 2–25.
5. Nakamura H, Jun F and Maeda H, Expert Opin. Drug Delivery, 2015, 12, 53–64.
6. Gref R, Minamitake Y, Peracchia MT, Trubetskoy V, Torchilin V and Langer R, Science, 1994, 263, 1600–1603. [PubMed: 8128245]
7. Moghimi SM, Hunter AC and Murray JC, Pharmacol. Rev, 2001, 53, 283–318. [PubMed: 11356986]
8. Danhier F, Feron O and Preat V, J. Controlled Release, 2010, 148, 135–146.
9. Davis ME, Chen Z and Shin DM, Nat. Rev. Drug Discovery, 2008, 7, 771–782. [PubMed: 18758474]
10. Byrne JD, Betancourt T and Brannon-Peppas L, Adv. Drug Delivery Rev, 2008, 60, 1615–1626.
11. Nicolas J, Mura S, Brambilla D, Mackiewicz N and Couvreur P, Chem. Soc. Rev, 2013, 42, 1147–1235. [PubMed: 23238558]

12. Anselmo AC, Prabhakarpandian B, Pant K and Mitragotri S, Transl. Mater. Res, 2017, 4, 014001.
13. Lee H, Dellatore SM, Miller WM and Messersmith PB, Science, 2007, 318, 426–430. [PubMed: 17947576]
14. Sileika TS, Barrett DG, Zhang R, Lau KHA and Messersmith PB, Angew. Chem. Int. Ed, 2013, 52, 10766–10770.
15. Ejima H, Richardson JJ, Liang K, Best JP, van Koeverden MP, Such GK, Cui J and Caruso F, Science, 2013, 341, 154–157. [PubMed: 23846899]
16. Hong S, Yeom J, Song IT, Kang SM, Lee H and Lee H, Adv. Mater. Interfaces, 2014, 1, 1400113.
17. Lee H, Scherer NF and Messersmith PB, Proc. Natl. Acad. Sci. U.S.A, 2006, 103, 12999–13003. [PubMed: 16920796]
18. Liu X, Cao J, Li H, Li J, Jin Q, Ren K and Ji J, ACS Nano, 2013, 7, 9384–9395. [PubMed: 24010584]
19. Park J, Brust TF, Lee HJ, Lee SC, Watts VJ and Yeo Y, ACS Nano, 2014, 8, 3347–3356. [PubMed: 24628245]
20. Abouelmagd SA, Meng FF, Kim BK, Hyun H and Yeo Y, ACS Biomater. Sci. Eng, 2016, 2, 2294–2303. [PubMed: 28944286]
21. Li J, Wu SX, Wu CC, Qiu LP, Zhu GZ, Cui C, Liu Y, Hou WJ, Wang YY, Zhang LQ, Teng IT, Yang HH and Tan WH, Nanoscale, 2016, 8, 8600–8606. [PubMed: 27050780]
22. Liu Y, Ai K, Liu J, Deng M, He Y and Lu L, Adv. Mater, 2013, 25, 1353–1359. [PubMed: 23280690]
23. Amin DR, Sugnaux C, Lau KHA and Messersmith PB, Biomimetics, 2017, 2, 17. [PubMed: 29360110]
24. Shin M, Lee H-A, Lee M, Shin Y, Song J-J, Kang S-W, Nam D-H, Jeon EJ, Cho M, Do M, Park S, Lee MS, Jang J-H, Cho S-W, Kim K-S and Lee H, Nat. Biomed. Eng, 2018, 2, 304–317.
25. Xiang S, Yang P, Guo H, Zhang S, Zhang X, Zhu F and Li Y, Macromol. Rapid Commun, 2017, **doi:** 10.1002/marc.201700446.**doi:**
26. Chen Z, Wang C, Chen J and Li X, J. Am. Chem. Soc, 2013, 135, 4179–4182. [PubMed: 23470166]
27. Zhang H, Yi Z, Sun Z, Ma X and Li X, J. Mater. Chem. B, 2017, 5, 7622–7631.
28. Pietta PG, J. Nat. Prod, 2000, 63, 1035–1042. [PubMed: 10924197]
29. Markham KR and Mabry TJ, phytochemistry, 1968, 7, 1197–1200.
30. Suh HJ, Lee JM, Cho JS, Kim YS and Chung SH, Food Res. Int, 1999, 32, 659–664.
31. Ju K-Y, Lee Y, Lee S, Park SB and Lee J-K, Biomacromolecules, 2011, 12, 625–632. [PubMed: 21319809]
32. Sunoqrot S, Bae JW, Jin SE, Pearson RM, Liu Y and Hong S, Bioconjugate Chem, 2011, 22, 466–474.
33. Cornard JP, Boudet AC and Merlin JC, Spectrochim. Acta, Part A, 2001, 57, 591–602.
34. Jokerst JV, Lobovkina T, Zare RN and Gambhir SS, Nanomedicine, 2011, 6, 715–728. [PubMed: 21718180]
35. Punnonen EL, Ryhanen K and Marjomaki VS, Eur. J. Cell Biol, 1998, 75, 344–352. [PubMed: 9628320]
36. Zhang C, Zhao X, Guo S, Lin T and Guo H, Int. J. Nanomedicine, 2017, 12, 1827–1840. [PubMed: 28331308]
37. Chen C-T, Martin-Martinez FJ, Jung GS and Buehler MJ, Chem. Sci, 2017, 8, 1631–1641. [PubMed: 28451292]
38. Hollman PCH and Arts ICW, J. Sci. Food Agric, 2000, 80, 1081–1093.
39. Biesaga M, J. Chromatogr. A, 2011, 1218, 2505–2512. [PubMed: 21411105]
40. Quideau S, Deffieux D, Douat-Casassus C and Pouységu L, Angew. Chem. Int. Ed, 2011, 50, 586–621.
41. Markova Z, Novak P, Kaslik J, Plachtova P, Brazdova M, Jancula D, Siskova KM, Machala L, Marsalek B and Zboril R, ACS Sustainable Chem. Eng, 2014, 2, 1674–1680.
42. Lee H, Rho J and Messersmith PB, Adv. Mater, 2009, 21, 431–434. [PubMed: 19802352]

43. Behzadi S, Serpooshan V, Tao W, Hamaly MA, Alkawareek MY, Dreaden EC, Brown D, Alkilany AM, Farokhzad OC and Mahmoudi M, Chem. Soc. Rev, 2017, 46, 4218–4244. [PubMed: 28585944]

44. Fernando LP, Kandel PK, Yu J, McNeill J, Ackroyd PC and Christensen KA, Biomacromolecules, 2010, 11, 2675–2682. [PubMed: 20863132]

45. Yameen B, Choi WI, Vilos C, Swami A, Shi J and Farokhzad OC, J. Controlled Release, 2014, 190, 485–499.

46. Zeng X, Morgenstern R and Nyström AM, Biomaterials, 2014, 35, 1227–1239. [PubMed: 24210875]

47. Kwon GS and Kataoka K, Adv. Drug Delivery Rev, 2012, 64, 237–245.

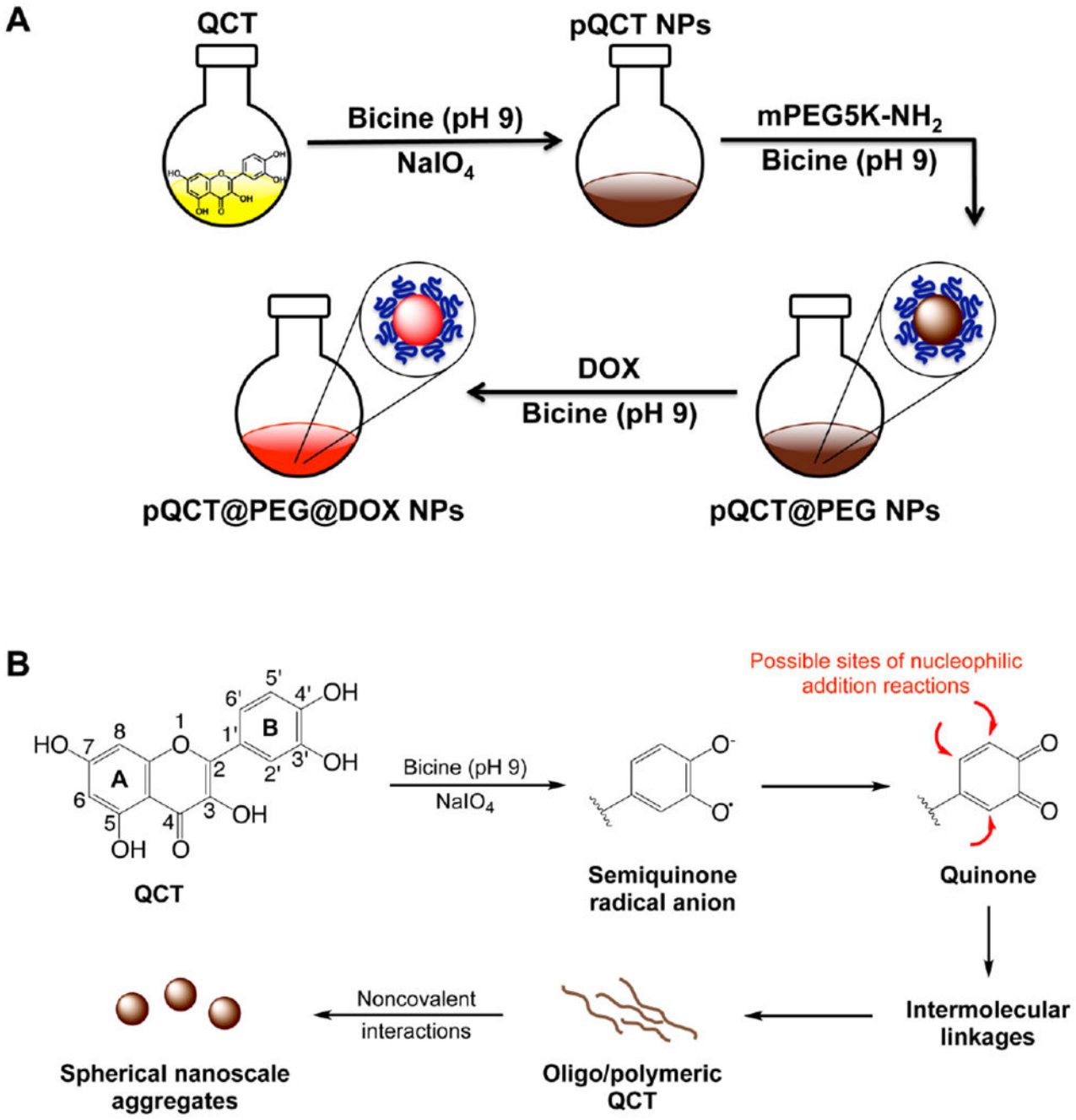

Figure 1.

(A) Overview of pQCT NP synthesis and subsequent modification with mPEG5K-NH_2 and DOX. (B) Proposed oxidative self-polymerization mechanism of QCT to form larger MW oligomers and colloidal aggregates stabilized by noncovalent interactions.

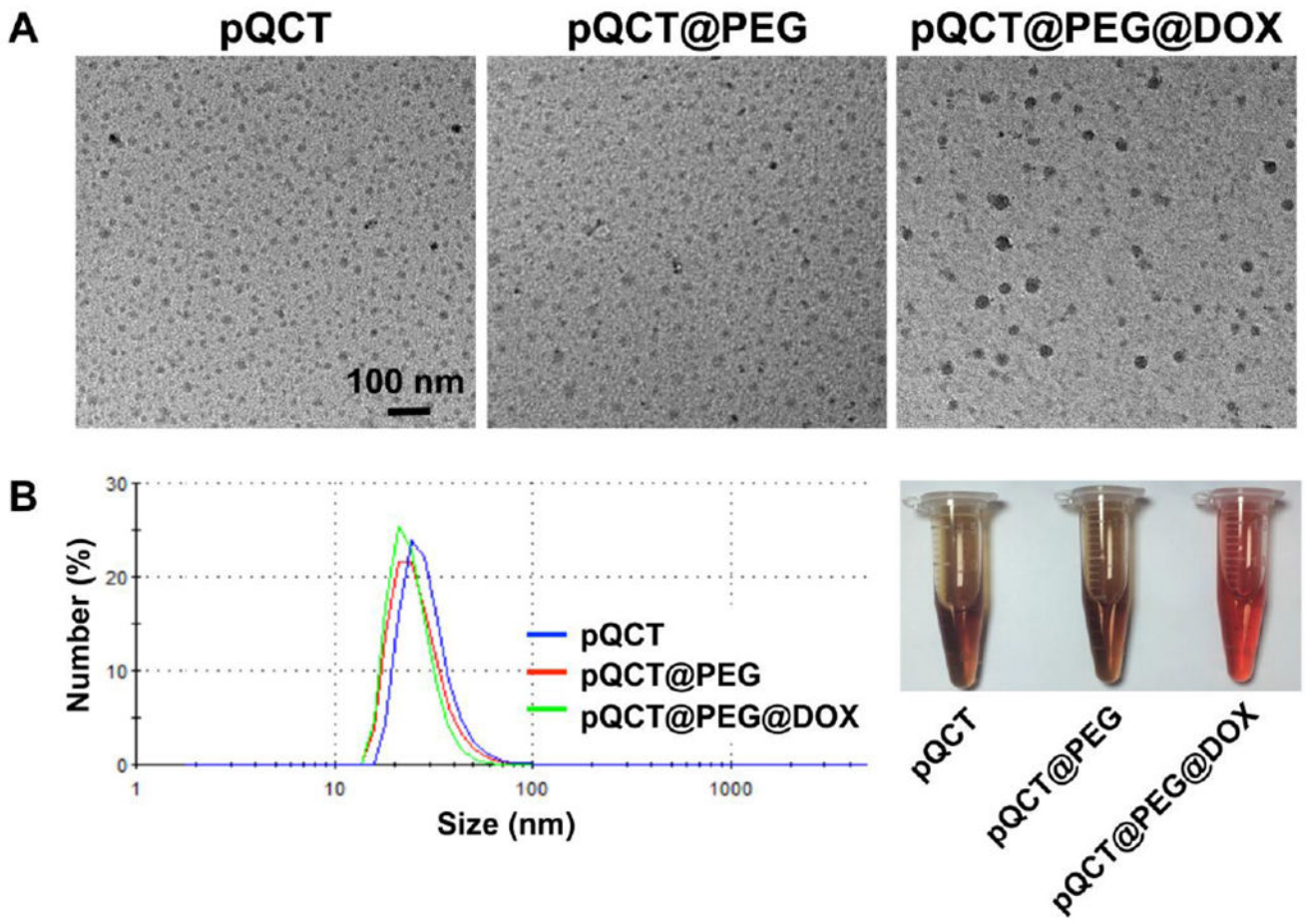

Figure 2.

QCT forms spherical water-dispersible NPs upon oxidative self-polymerization, which were sequentially functionalized with mPEG5K-NH_2 and DOX. (A) Representative TEM images and (B) particle size distributions by DLS of pQCT, pQCT@PEG, and pQCT@PEG@DOX NPs dispersed in MilliQ water.

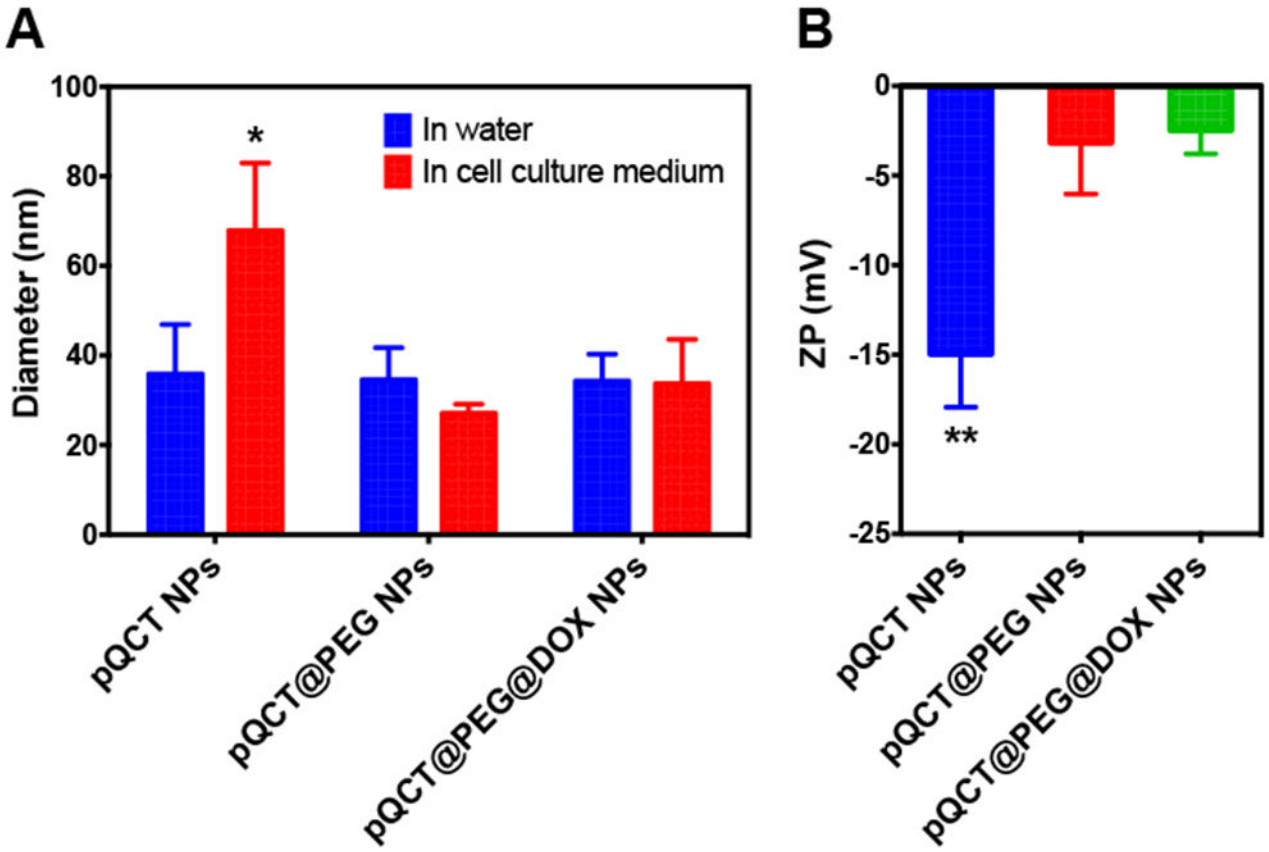

Figure 3.

Characterization of unmodified and modified pQCT NPs by DLS and zeta potential measurements. (A) Particle size of pQCT NPs is not significantly changed after PEGylation and DOX incorporation. Around 2-fold increase in size ($p < 0.05$) is observed upon incubation of pQCT NPs in cell culture medium supplemented with 10% FBS, while PEGylated NPs maintained steric stability. Results represent the mean ± SD from three different batches of NPs. (B) Zeta potential of pQCT NPs is significantly increased ($p < 0.01$) after PEGylation, verifying surface modification with PEG. Results represent the mean ± SD from three different batches of NPs.

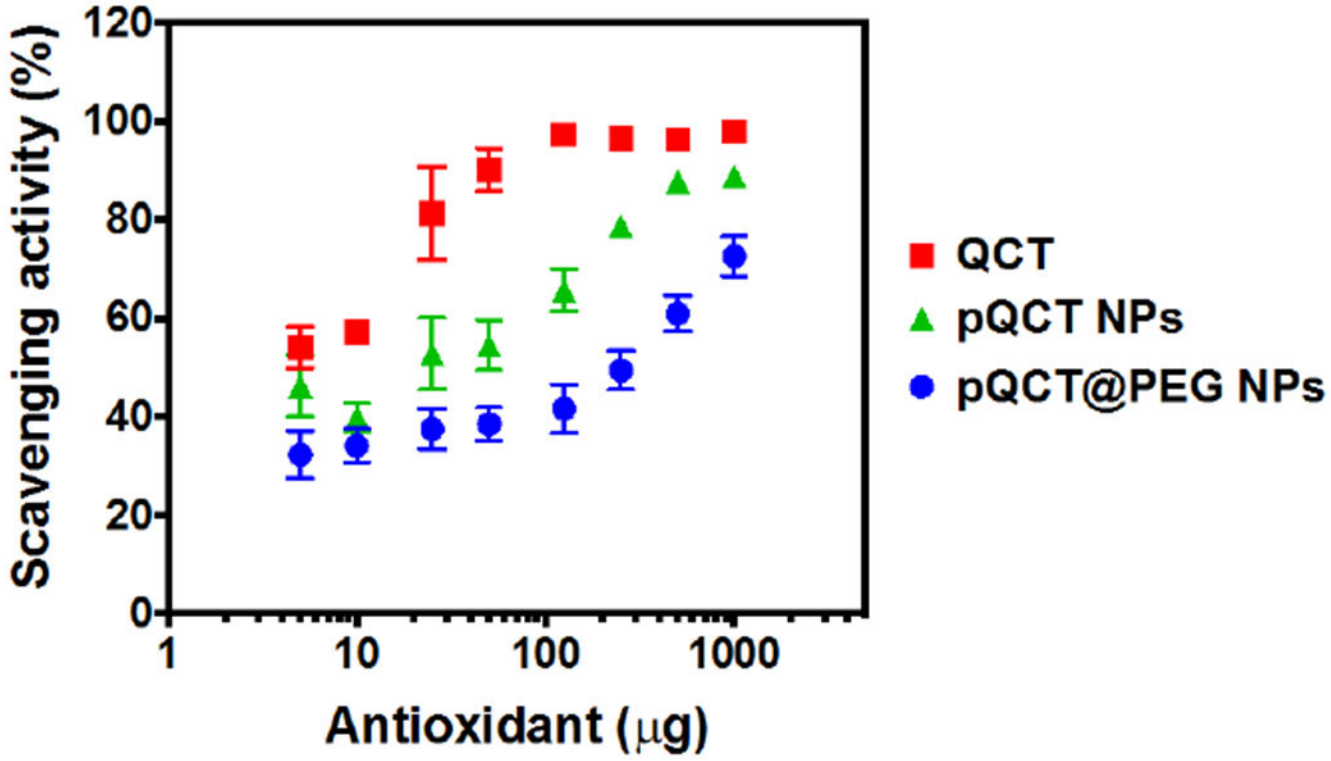

Figure 4.

Antioxidant activity of pQCT and pQCT@PEG NPs compared to unmodified QCT expressed as % DPPH radical scavenging activity. Although reduced, antioxidant activity of pQCT and pQCT@PEG NPs is still present. Results are expressed as mean ± SD from three different batches of NPs.

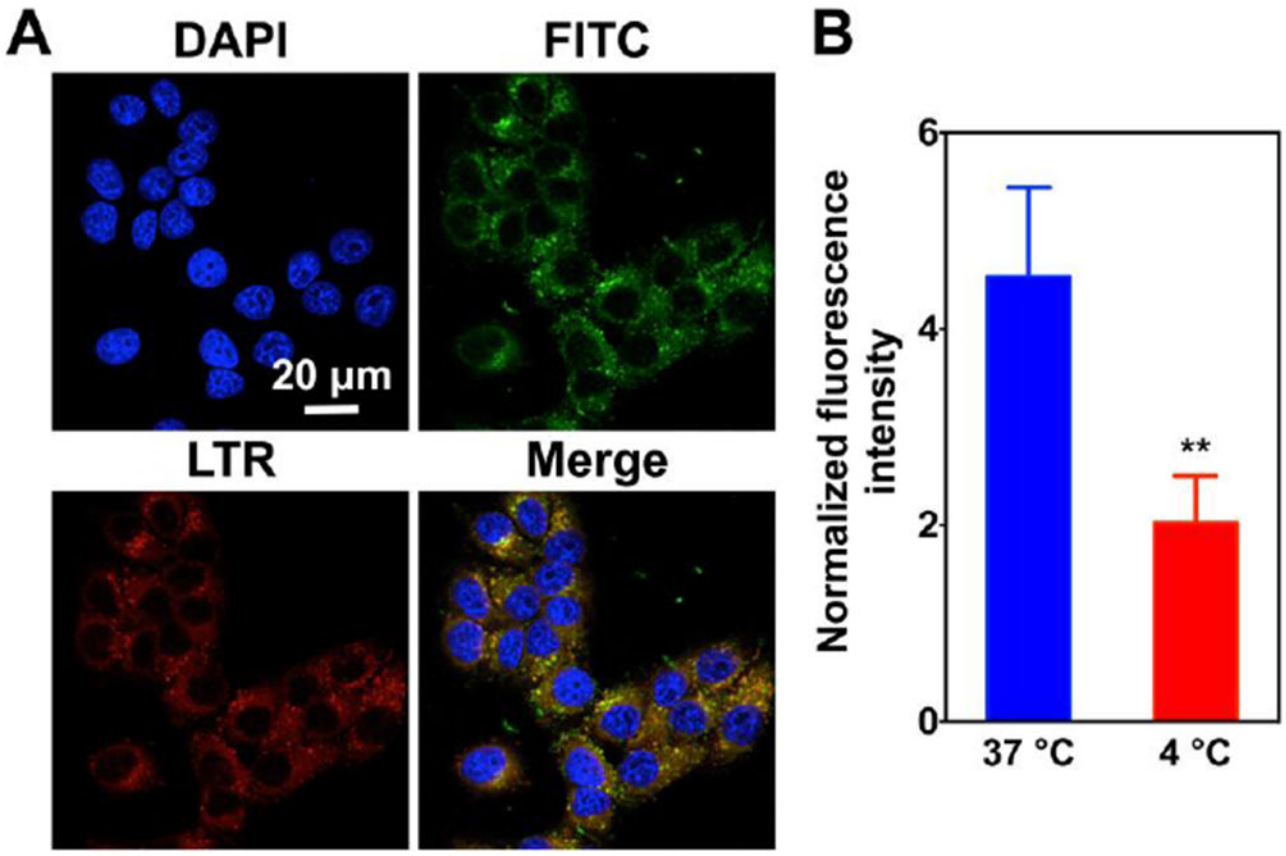

Figure 5.

Endo-lysosomal uptake of pQCT@FITC-PEG NPs by KB cells. (A) CLSM images of KB cells incubated with 10 μg/mL pQCT@FITC-PEG NPs for 24 h (blue channel: cell nuclei stained with DAPI; green channel: FITC-labeled NPs; red channel: LTR). Colocalization of green (FITC-labeled NPs) and red (LTR) fluorescence signals (Pearson's correlation coefficient = 0.71) indicates the presence of the NPs in lysosomal compartments. (B) Uptake of pQCT@FITC-PEG NPs by KB cells is significantly reduced ($p < 0.01$) after incubation at 4 °C for 3 h, confirming an endo-lysosomal uptake pathway. Results are plotted as mean ± SD of cell-associated fluorescence intensity relative to unstained cells measured by flow cytometry from three independent experiments.

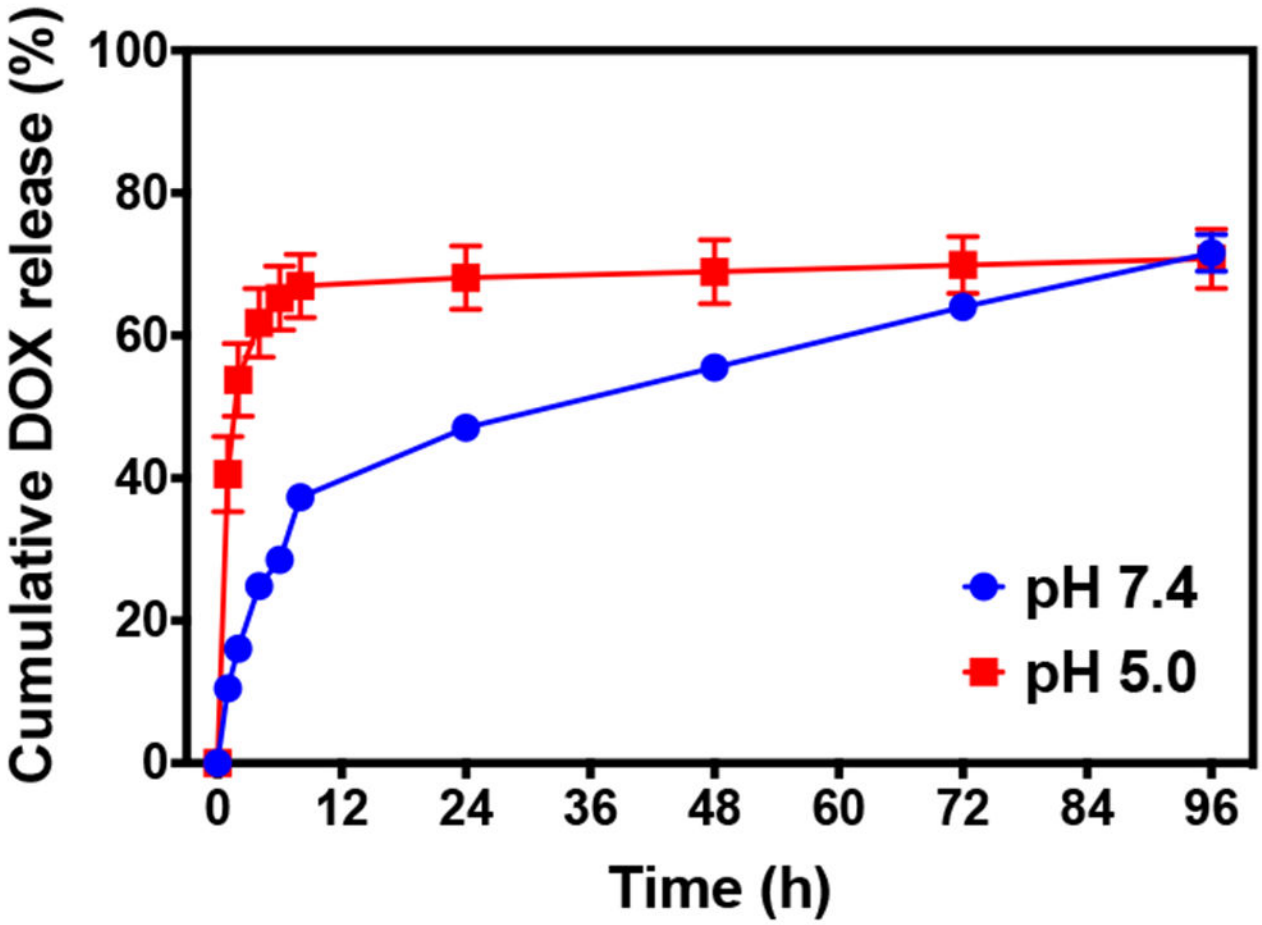

Figure 6.

Slow and sustained release of DOX from pQCT@PEG@DOX NPs up to 4 days in PBS (pH 7.4) and acetate buffer (pH 5.0). Release at pH 5.0 was faster than pH 7.4. Results are plotted as mean ± SD of the % cumulative amount of DOX released over time from triplicate samples.

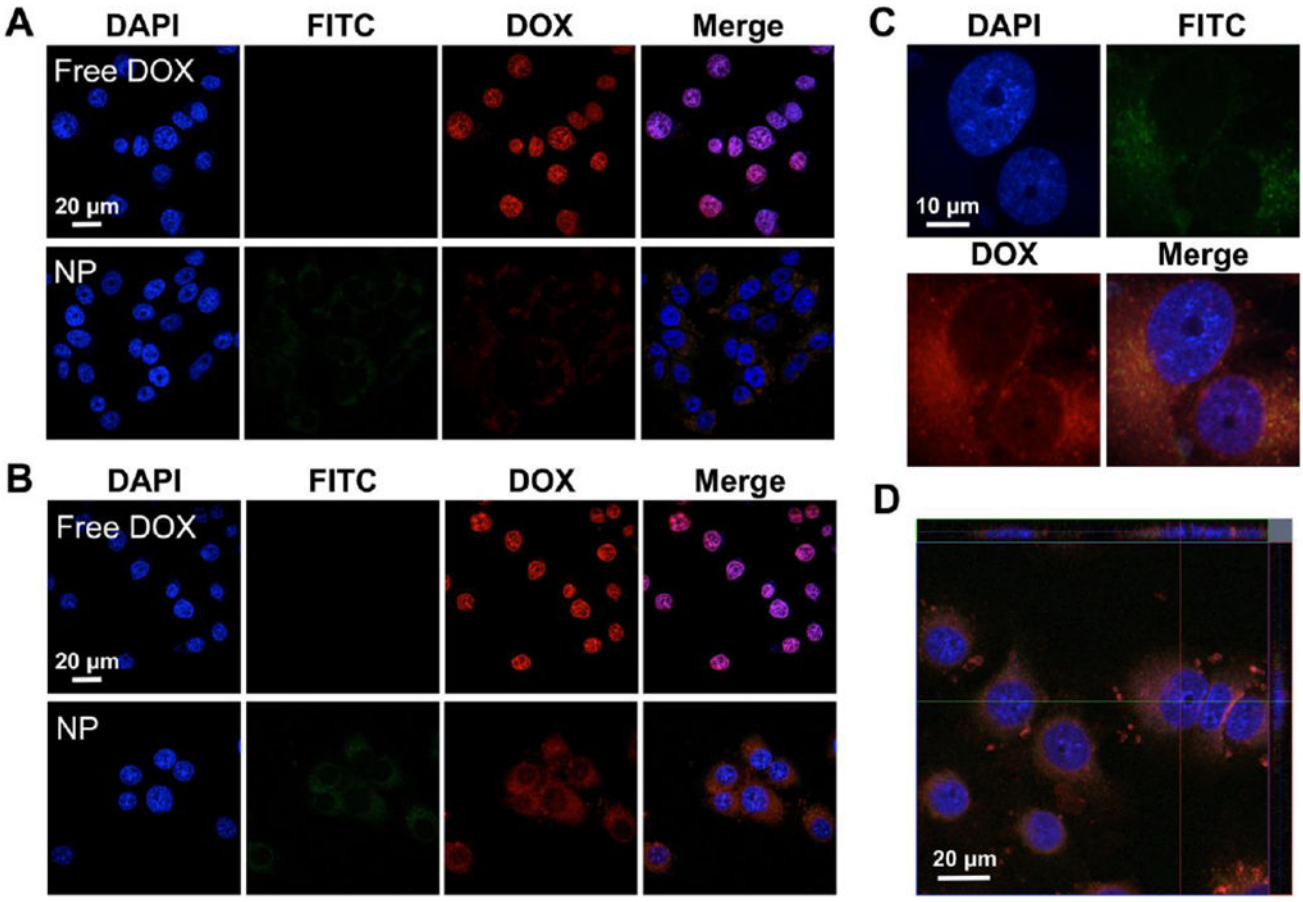

Figure 7.

Time dependent cellular uptake of DOX from pQCT@FITC-PEG@DOX NPs in KB cells compared to free DOX (blue channel: cell nuclei stained with DAPI; green channel: FITC-labeled NPs; red channel: DOX). (A) CLSM images of KB cells after 3 h incubation with 5 μM free DOX and DOX-loaded NPs showing strong nuclear red fluorescence signals for free DOX but not the NPs due to insufficient drug release. (B) CLSM images of KB cells after 24 h incubation show nuclear localization of DOX upon its release from pQCT@FITC-PEG@DOX NPs. (C) Enlarged image and (D) orthogonal view of KB cells incubated with pQCT@FITC-PEG@DOX NPs for 24 h showing nuclear localization of DOX.

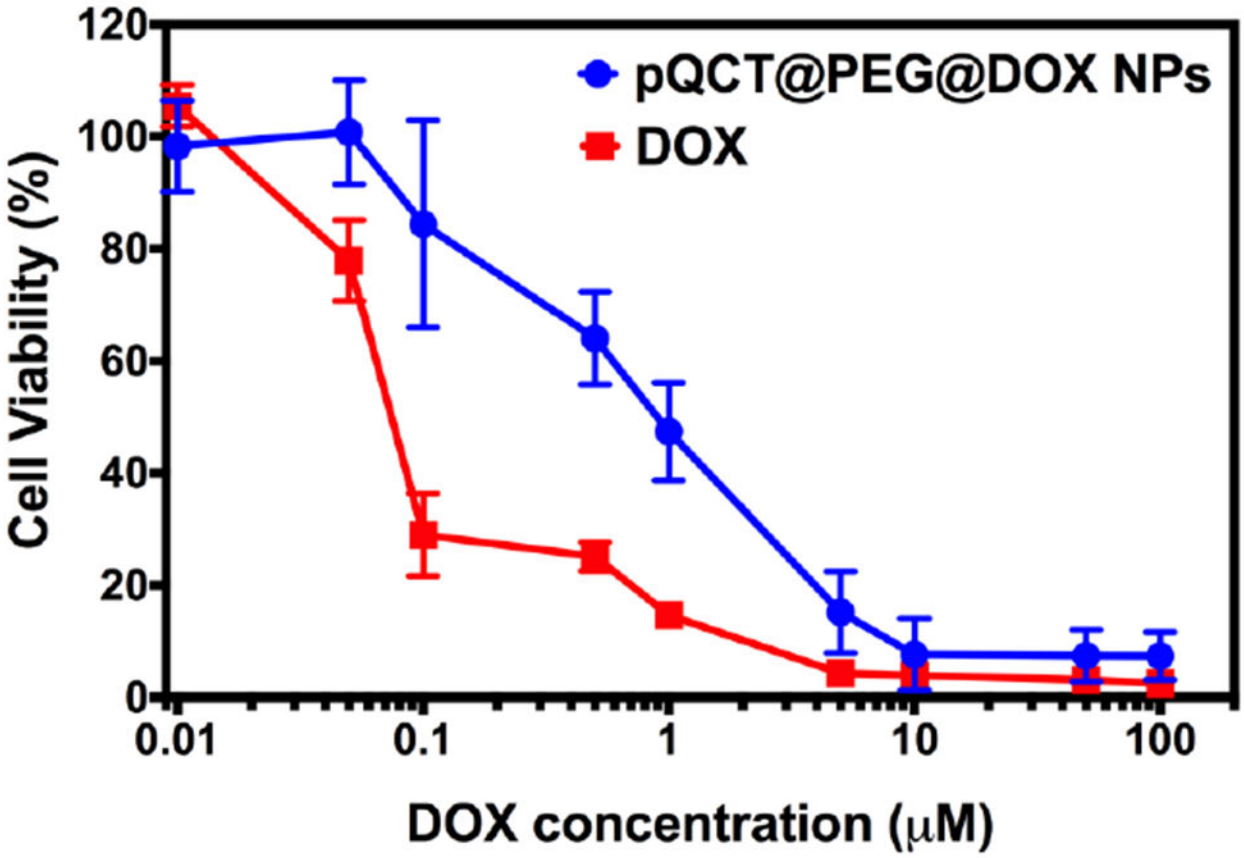

Figure 8.

Viability of KB cells incubated with free DOX or DOX-loaded NPs at DOX concentrations ranging from 0 to 100 μM in complete RPMI 1640 for 48 h. Results are plotted as mean ± SD of % cell viability obtained from three independent experiments. IC50 for the two groups was determined by fitting the data into a dose-response curve using Graphpad Prism 6.0e.

Table 1.

Surface elemental composition of unmodified and modified pQCT NPs obtained from XPS high resolution scans of the C 1s, O 1s, and N 1s regions. Results are expressed as mean ± SD from scanning three different regions for each sample.

NP	C (%)	O (%)	N (%)	C/O
pQCT	68.0 ± 3.3	31.6 ± 3.4	0.3 ± 0.2	2.15
pQCT@PEG	64.2 ± 2.9	34.7 ± 2.9	1.2 ± 0.1	1.85
pQCT@PEG@DOX	61.0 ± 0.4	37.4 ± 0.8	1.6 ± 0.4	1.63